


WaveFlex biosensor based on S-tapered and waist-expanded technique for detection of glycosylated hemoglobin

GUIWEI ZHANG,¹ RAGINI SINGH,² BINGYUAN ZHANG,¹ SANTOSH KUMAR,^{1,*}  AND GUORU LI^{1,3}

¹Shandong Key Laboratory of Optical Communication Science and Technology, School of Physics Science and Information Technology, Liaocheng University, Liaocheng 252059, China

²College of Agronomy, Liaocheng University, Liaocheng 252059, China

³guoruli@lcu.edu.cn

*santosh@lcu.edu.cn

Abstract: Glycosylated hemoglobin (HbA1c) is considered a new standard for the detection of diabetes mellitus because it is more accurate than regular blood sugar tests and there is no need to take blood on an empty stomach or at a specific time. In this work, we have developed a novel optical fiber biosensor, referred to as the “WaveFlex biosensor,” which operates on the principles of localized surface plasmon resonance (LSPR) plasmonic wave. The sensor is fabricated using an innovative S-tapered and waist-expanded technique, enabling it to effectively detect HbA1c. Compared to the HbA1c sensors currently in use, HbA1c optical fiber sensors possess the characteristics of high sensitivity, low cost, and strong anti-interference ability. The gold nanoparticles (AuNPs), cerium oxide (CeO₂) nanorods (NRs), and tungsten disulfide (WS₂) nanosheets (NSs) are functionalized to improve the effectiveness of the fiber sensor on the probe surface. AuNPs are utilized to generate LSPR by the excitation of evanescent waves to amplify the sensing signal. The CeO₂-NRs can have a strong metal-carrier interaction with AuNPs, enhancing the cascade of CeO₂-NRs and AuNPs. The WS₂-NSs with layered fold structure have a large specific surface area. Therefore, the combination of CeO₂-NRs and WS₂-NSs is conducive to the binding of antibodies and the addition of sites. The functionalized antibodies on the fiber make the sensor probe capable of specific selection. The developed probe is applied to test the HbA1c solution over concentrations of 0–1000 µg/mL, and the sensitivity and limits of detection of 1.195×10^{-5} a.u./µg/mL and 1.66 µg/mL are obtained, respectively. The sensor probe is also evaluated using assays for reproducibility, reusability, selectivity, and pH. According to the findings, a novel method for detecting blood glucose based on a plasmonic biosensor is proposed.

© 2023 Optica Publishing Group under the terms of the [Optica Open Access Publishing Agreement](#)

1. Introduction

Hyperglycemia is a defining feature of the metabolic illness. Diabetes mellitus (DM) is one of the top ten global causes of death for people [1]. DM usually does not cause serious damage, but persistent hyperglycemia can result in many dangerous complications. These complications can lead to a coma or even death if left untreated. Eye, kidney, nerve, heart, and blood vessel problems are the most common long-term consequences of DM [2–4]. Early blood glucose management has been proven to be an effective means to prevent or delay DM-related complications [5]. As a biomarker for the clinical diagnosis and management of DM, glycosylated hemoglobin (HbA1c) is considered to be the most valuable indicator of glycemic control status [6,7]. The N-terminal valine residues of the hemoglobin β-chain and glucose combine to generate the stable molecule known as HbA1c. The degree of glycosylation depends on the time of protein contact with blood glucose and the concentrations [8]. Compared with the regular blood glucose index, the HbA1c

index is more stable and unaffected by the testing time, fasting insulin injection, or hypoglycemic drugs. The HbA1c index can reflect the average blood glucose level in the past 2-3 months with good stability [9]. As it currently stands, the level of HbA1c in the human body is considered normal if it is below 6.5% [10]. If the measured value is higher than the standard, it can be considered pre-DM or has developed DM. For the diagnosis and treatment of DM and insulin resistance, the measurement of HbA1c is crucial [11,12].

Luminescence, electrochemistry, and colorimetry are among the biosensors for detecting HbA1c [13,14]. To measure HbA1c, Ahn *et al.* created a luminol chemiluminescence biosensor based on a gold substrate treated with boronic acid. The constructed biosensor's linear dynamic range of HbA1c was good, ranging from 2.5% to 17.0%, covering the entire range of clinically significant levels [15]. Thapa *et al.* created a label-free, single-sample electrochemical detection technique for glucose and HbA1c based on altering carbon electrodes. The results demonstrated that the sensitivity of the biosensor was $0.09 \mu\text{Amm}^{-2}\mu\text{g}^{-1}$ [16]. Mulder *et al.* utilized the colorimetry method to detect fructose-based amino acids to indirectly detect HbA1c in blank serum doped with fructose-based amino acids. The results showed that the spectrophotometric readings and colorimetric results could be obtained by visual detection [17]. However, the biosensors based on the above methods have the disadvantages of poor long-term performance stability and complex system assembly [18]. The optical fiber biosensors have the advantages of high sensitivity and portability. The detection of proteins, viruses, bacteria, and DNA has been made possible by label-free testing and robust anti-interference abilities [19–23]. There is no application of optical fiber biosensors in the detection of HbA1c. It is very necessary to explore the potential of optical fiber biosensors in the detection of HbA1c.

Different optical fiber sensing technologies are used to measure various quantities [24–26], of which Localized surface plasmon resonance (LSPR) is one with excellent performance. LSPR is a kind of technology that utilizes an electromagnetic field to excite the electron collective oscillation of metal atoms on the probe surface to realize signal enhancement. The LSPR fiber sensors possess higher sensitivity, lower cost, and better environmental stability [21]. The special fiber structures and nanoparticles (NPs) immobilized on the fiber are usually utilized to enhance the signal of LSPR fiber sensors. For the detection of creatinine, Li *et al.* suggested a sensitive fiber biosensor based on single mode fiber-multicore fiber-multimode fiber-single mode fiber (SMF-MCF-MMF-SMF). Graphene oxide and MoS_2 -NPs were used to modify the fiber probe to increase the binding site of biomolecules, and creatinine detection with a sensitivity of $2.5 \text{ pm}/\mu\text{M}$ was realized [18]. To detect glucose in the human body, Feng *et al.* created an LSPR fiber biosensor based on a monolayer graphene/AuNPs three-dimensional hybrid structure, attaining a sensitivity of $1317.61 \text{ nm}/\text{RIU}$ [27].

CeO_2 -NPs possess the advantages of fine particle size, large surface area, high biochemical activity, and good optical properties and have been widely used in gas detection, photocatalysis, and fuel cell particle thin films [28–30]. Moreover, CeO_2 -NPs have been prepared into heterojunction structures with other materials and applied in the biosensors field, showing good cascading ability with other low-dimensional materials. In order to achieve the ultrasensitive detection of enolase that is specific to neurons, Li *et al.* devised a luminol-based electrochemiluminescence (ECL) biosensor. With a LOD of 72.4 fg/mL , the proposed ECL immunosensor based on $\text{CePO}_4/\text{CeO}_2$ heterostructures was able to detect substances with high sensitivity in the detection range of 76 fg/mL - 100 ng/mL [31]. Based on a $\text{CeO}_2/\text{MXene}$ heterojunction and a configuration-entropy-driven dual-toehold strand displacement reaction for signal amplification, Cheng *et al.* created an ECL biosensing platform to identify the BCR-ABL fusion gene. The LOD was as low as 0.27 fM , and the designed ECL biosensor accomplished a broad concentration variation from 1 fM to 100 pM [32]. With exceptional physical and chemical characteristics, a very high specific surface area, strong biocompatibility, and minimal cytotoxicity, WS_2 is a great material that has been applied in biosensors and photosensitive therapy [33]. The layered fold structure of WS_2 gives its a large

specific surface area, which is beneficial to the attachment of biomolecules. In this work, AuNPs, CeO₂-NRs, and WS₂-NSs were immobilized on the fiber probe. CeO₂ is often employed to stabilize and disperse the metal particles on the load, generating a strong metal-carrier interaction and enhancing the cascade of CeO₂-NRs and AuNPs [34]. A compact integrated composite structure can be formed on the surface of the fiber probe by combining CeO₂-NRs and WS₂-NSs.

In this work, a highly sensitive biosensor based on plasmonics, the S-tapered and waist-expanded technique, was developed for the detection of HbA1c. The fiber probe based on micro-processing techniques can have a high sensitivity to refractive index (RI) changes. AuNPs, CeO₂-NRs, and WS₂-NSs were sequentially immobilized on the probe to improve the effectiveness of sensing and expand the antibody sites. By functionalizing HbA1c antibodies on the probe surface, the proposed probe possesses the ability to detect HbA1c specifically. Here, the prepared plasmonic biosensor was utilized to measure HbA1c solutions over a linear range of 0-1000 µg/mL. Additionally, the reusability, reproducibility, stability, pH test, and selectivity tests were performed to assess the application in real life.

2. Experiments

2.1. Materials

The fiber probe based on the S-tapered and waist-expanded technique was made by SMF (8.2 µm, 125 µm) from EB-link Technologies Co., Ltd., China. AuNPs were synthesized by the following reagents: trisodium citrate, hydrogen tetrachloroaurate, and deionized (DI) water. CeO₂-NRs and WS₂-NSs were purchased from Nanjing XFNANO Materials Tech Co., Ltd, China. DI water and N-methylpyrrolidone were used to dissolve CeO₂-NRs and WS₂-NSs, respectively. Acetone, concentrated sulfuric acid (H₂SO₄, 98%), hydrogen peroxide solution (H₂O₂, 30%), and ethanol were utilized to clean the fiber. For the immobilization of nanomaterials, (3-mercaptopropyl)trimethoxysilane (MPTMS) was used. The functionalization of antibodies was accomplished with the help of N-hydroxy succinimide (NHS), 1-(3-dimethylaminopropyl)-3-ethylcarbodiimide hydrochloride (EDC), and 11-mercaptoundecanoic acid (MUA). HbA1c antibodies and HbA1c were both from Cloud-Clone Corp, China. Several biological reagents, such as myoglobin, bovine blood protein (BBP), bovine serum albumin (BSA), and glucose, were purchased from Macklin (Shanghai) for the selectivity test.

2.2. Instruments and measurements

The fiber structure based on the S-tapered and waist-expanded technique was fabricated by using the 3SAE combiner manufacturing system (CMS) and a special fusion splicer machine (FSM-100P+, Fujikura) in combination. Scanning electron microscopy (SEM) utilized a fine focused electron beam to scan the surface of the samples to characterize the fiber structure and the nanomaterials functionalized on the fiber surface. The microstructure of nanomaterials was analyzed by high-resolution transmission electron microscopy (HR-TEM, Talos L120C, Thermo Fisher Scientific). The absorption spectrum of AuNPs was tested by a UV-visible spectrophotometer. The tungsten-halogen light source (HL-2000, Ocean Optics) was employed as the excitation light source, and a spectrometer (USB2000+, Ocean Optics) was used to record the spectrum through the transmitted intensity experiment.

2.3. Preparation of sensor probe

The fiber probe was fabricated from conventional SMF. The fabrication process of the fiber probe was shown in Fig. 1(a). Firstly, the FSM was utilized to fabricate the spherical structure by controlling the amount of overlap during fusing, as shown in Fig. 1(b). Under normal circumstances, there was no fiber diameter change at the fusion splices after the fusion was completed. When the amount in overlap during fusing progress was set to 20 µm, both ends of

the fiber were fused properly. With the increase of overlap, the fusion splices of fiber exhibited a spherical structure after fusing, and the size of the spherical diameter got larger with the increase in overlap. If the diameter of the ball is too large, the transmitted spectrum intensity will be too low, which is not conducive to subsequent sensing experiments. Finally, the amount of overlap was set to a preset maximum of $100\ \mu\text{m}$, corresponding to the ball diameter of $150\ \mu\text{m}$. After the fabrication of the spherical fiber structure, a distance of $600\ \mu\text{m}$ was selected at the right side of the spherical structure to fabricate a S-taper. The distance of $600\ \mu\text{m}$ can prevent the spherical structure from being affected during the tapering process. As shown in Fig. 1(c), the S-taper was prepared by the optimizer in the CMS, and finally, the sensor based on the S-tapered and waist-expanded techniques was obtained.

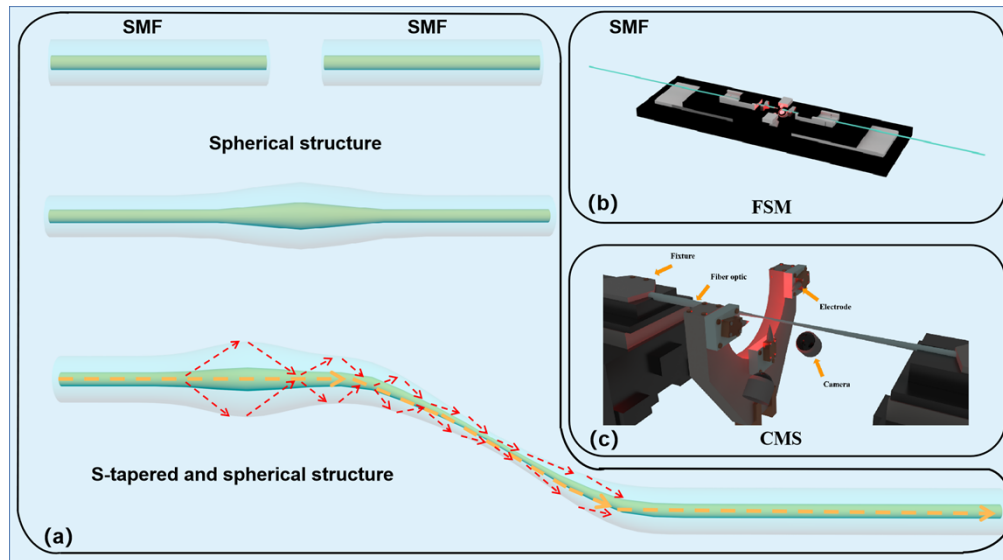


Fig. 1. (a) The fabrication process of sensor probe, (b) fusion splicer machine (FSM), (c) combiner manufacturing system (CMS).

2.4. Sensing principle and stimulation

The RSoft software was utilized to simulate the fiber structure based on the S-tapered and waist-expanded techniques. Firstly, the S-tapered fibers with diameters of $40\ \mu\text{m}$, $60\ \mu\text{m}$, and $80\ \mu\text{m}$ were simulated, as shown in Fig. 2. The S-tapered fiber structure of $40\ \mu\text{m}$ has a lower transmission intensity, meaning that it can generate stronger EWs. As can be seen from Fig. 2(a), the fundamental mode is coupled to the cladding at the first bending position of the S-taper to form the higher-order mode, and the higher-order modes in the cladding at the second bending position after propagation for some distance are coupled to the core. On this basis, the light field variations of spherical and S-tapered cascaded structures with different diameters are simulated, respectively. The results of Fig. 3 show that the light field distribution is not obviously different from that of a single S-taper fiber structure when the spherical diameter of the sphere is less than $150\ \mu\text{m}$.

As shown in Fig. 3(a), it can be clearly seen that the light in the core is coupled to the cladding after passing through the spherical structure when the diameter of the spherical structure is $150\ \mu\text{m}$, optimizing the defect of insufficient light field energy in the cladding of the front part of the S-taper. Compared with the straight-taper fiber structure, the S-tapered fiber structure can generate stronger EWs under light excitation and enhance the interaction between light and the

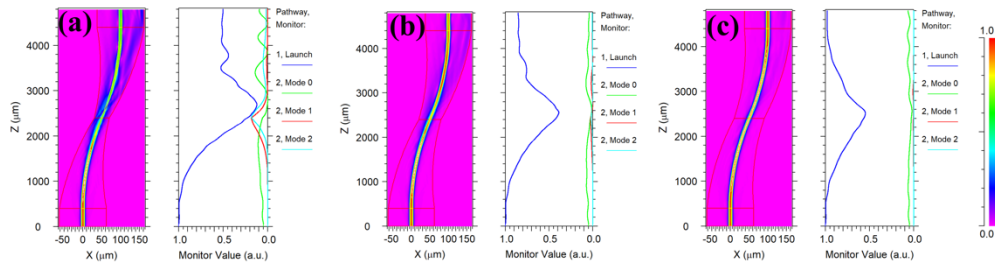


Fig. 2. Simulation results of an S-tapered fiber structure with different diameters. (a) 40 μm , (b) 60 μm and (c) 80 μm .

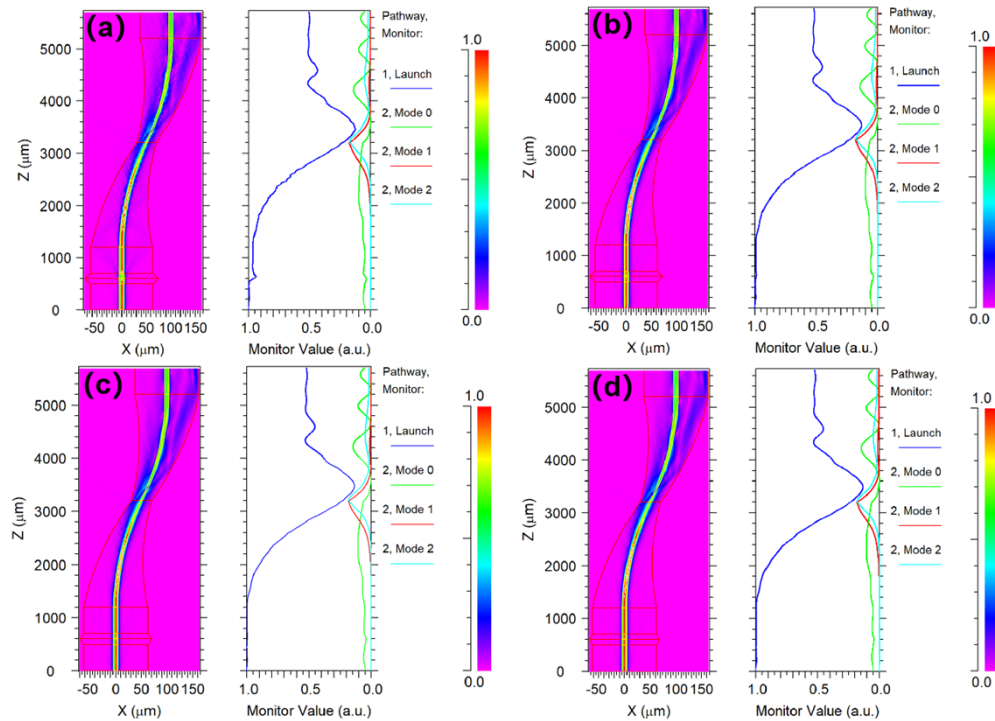


Fig. 3. Simulation results of an S-taper-based spherical structure with different cladding diameters: (a) 150 μm , (b) 145 μm , (c) 140 μm , and (d) 135 μm .

object to be measured. The S-tapered fiber has the characteristics of temperature insensitivity, fast response speed, and high sensitivity [35]. The spherical structure of the front end of the S-taper can make up for the deficiency of light field energy in the front cladding of the S-taper. Therefore, the combination of the two fiber structures can make the fiber have a good sensing response. The fiber structure based on the S-tapered and waist-expanded technique can produce more EWs, which are more sensitive to the RI of the external environment and are conducive to sensing applications.

2.5. Nanomaterials and antibodies functionalization

To ensure that the fiber surface is sufficiently clean, acetone was used to clean the fiber probe sensing area to remove most of the organic dust. The dry fiber probe was engulfed in Piranha solution ($\text{H}_2\text{O}_2:\text{H}_2\text{SO}_4 = 3:7$) for 30 minutes. This procedure created a hydroxyl layer on the

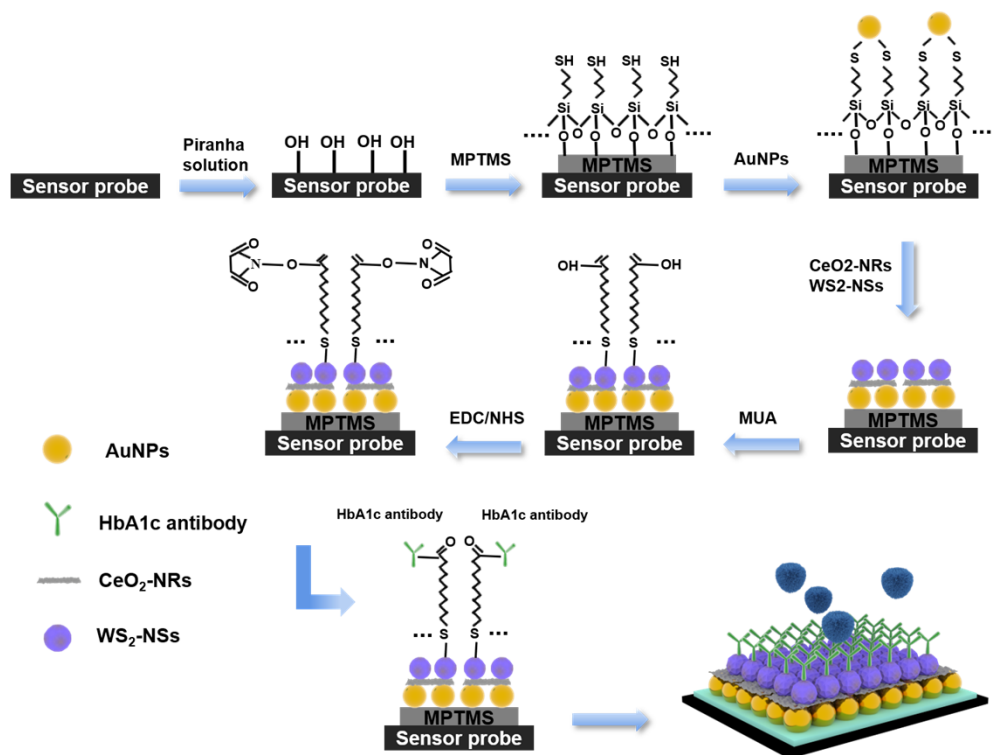


Fig. 4. Schematic of the NPs-immobilization and HbA1c antibody-functionalization process.

probe surface. To get rid of the remainder Piranha solution, the probe was cleaned with DI water and dried at 70 °C. The entire functionalization process of the probe is shown in Fig. 4. The immobilization of AuNPs was completed by the method of covalent bond. Firstly, the sensor probe was engulfed in ethanol containing MPTMS for 12 hours to modify the SH group of the sensing region. Then, the sensing region was immersed in AuNPs solution for 48 hours, and the MPTMS mercaptan groups and AuNPs formed a stable covalent connection, which was conducive to the adhesion of AuNPs to the probe surface. To make CeO₂-NRs solution, 17 mL of NMP solution was mixed with 8 mg of CeO₂-NRs powder. The mixture was evenly dispersed by ultrasonic treatment for one hour. And the supernatant was obtained by centrifugation at 3000 rpm for 15 min to complete the process of functionalization [36]. 1 mg of WS₂ powder was dissolved in DI water, and the WS₂-NSs solution was obtained by the same method [33]. CeO₂-NRs and WS₂-NSs were successive immobilized on the surface of the fiber sensing area by the annealing method.

HbA1c antibodies were functionalized on the nanomaterial surface by amino-conjugated fixation, which could produce high-quality results. To permanently fix the carboxylic base on the probe surface, the probe was first submerged in a 5 mL, 0.5 mM MUA ethanol solution for 5 hours. The carboxyl group was then activated to generate an amine-active lipid using a combination of 5 mL of EDC (200 mM) and 5 mL of NHS (50 mM).

The specific method was dipping the probe in the solution for 30 minutes. Finally, the sensor probe was functionalized with HbA1c antibodies by immersing it in an antibody solution (20 µg/mL) for 12 hours to achieve a specific selection of the sensor probe [37]. The 10 mg/mL of BSA solution was utilized to block the unreacted sites and minimize nonspecific adsorption. The transmitted intensity before and after functionalization is compared, and the results are shown

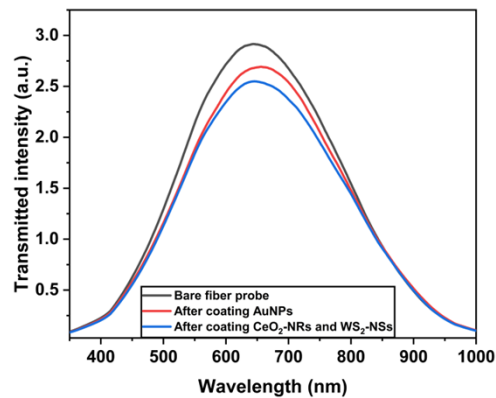


Fig. 5. The comparison of transmitted intensity between bare fiber probe and fiber with functionalization.

in Fig. 5. It can be seen that the transmitted intensity decreases after the functionalization of AuNPs and nanomaterials.

2.6. Preparation of HbA1c solutions

The 1×PBS solution was used to prepare HbA1c solutions with concentrations of 0, 10, 50, 200, 400, 600, and 1000 $\mu\text{g/mL}$. The specific method was used to prepare a concentration of 1000 $\mu\text{g/mL}$ of HbA1c solution. After that, 1×PBS solution was utilized to dilute and obtain the required low-concentration of HbA1c solution. Different concentrations of HbA1c solutions were applied to test the sensing capabilities of the developed probe.

2.7. Experimental setup

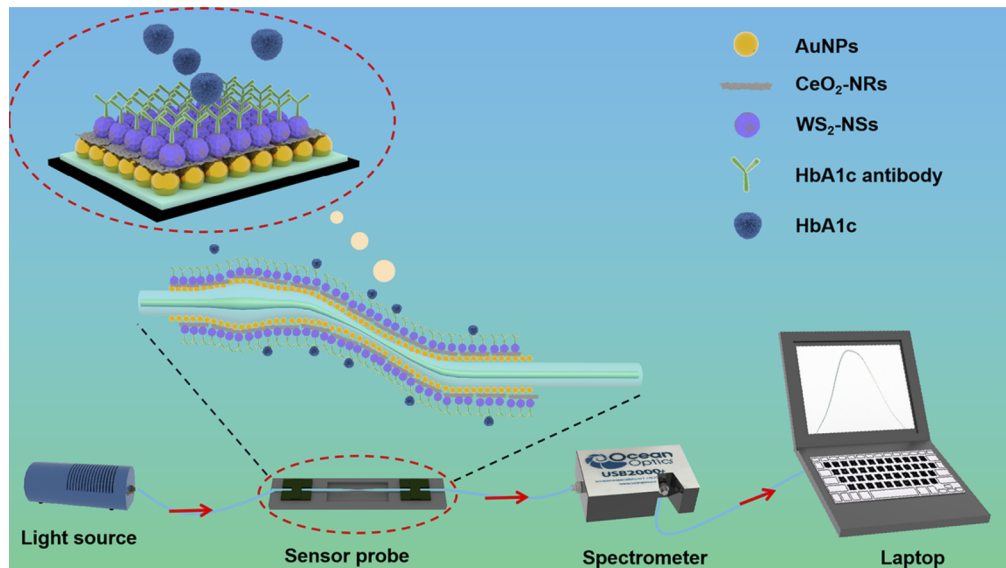


Fig. 6. Schematic of the experimental setup for detection of HbA1c.

The schematic diagram of the experimental setup for measuring the HbA1c solution is shown in Fig. 6. The halogen light source with a band of 200-1000 nm was employed to excite AuNPs immobilized on the probe to generate LSPR. The spectrum generated by the probe under the action of the light field was recorded by the spectrometer and transmitted to the laptop. The concentration change of the HbA1c solution can be analyzed through the transmitted intensity on the computer.

3. Results and discussions

3.1. Characterization of fiber structure and nanomaterials

A UV-visible spectrophotometer was used to determine the absorption spectrum of AuNPs, as shown in Fig. 7(a), and its absorption peak wavelength is located at 520 nm. Figure 7(b) showed the HR-TEM information of AuNPs; the size of AuNPs was relatively uniform (about 10 nm). The size of the AuNPs corresponded exactly to the measured peak wavelength of absorption. HR-TEM information of CeO₂-NRs was shown in Fig. 7(c), from which an obvious compact rod-like structure could be seen. Figure 7(d) displays HR-TEM images of WS₂-NSs, and the obvious layered fold structure can be observed from the picture, which was confirmed by previous work [38]. The combination of CeO₂-NRs and WS₂-NSs was beneficial to improving the performance of sensor probes.

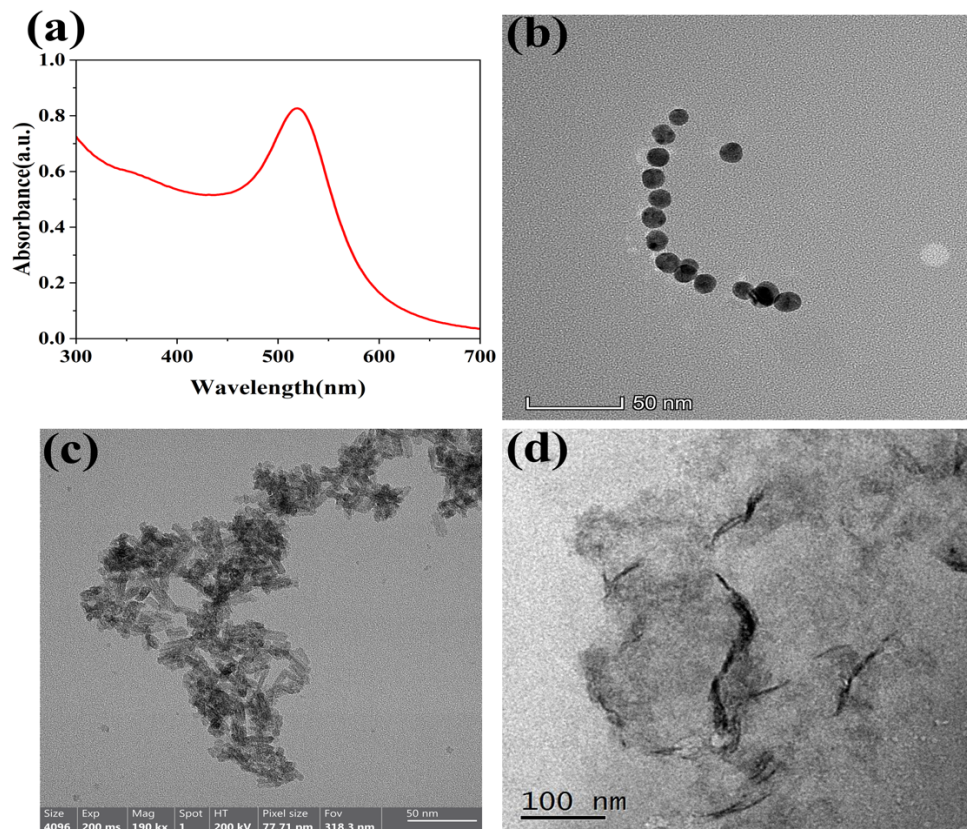


Fig. 7. (a) Absorbance spectrum of AuNPs, (b) HR-TEM image of AuNPs, (c) HR-TEM images of CeO₂-NRs and (d) WS₂-NSs.

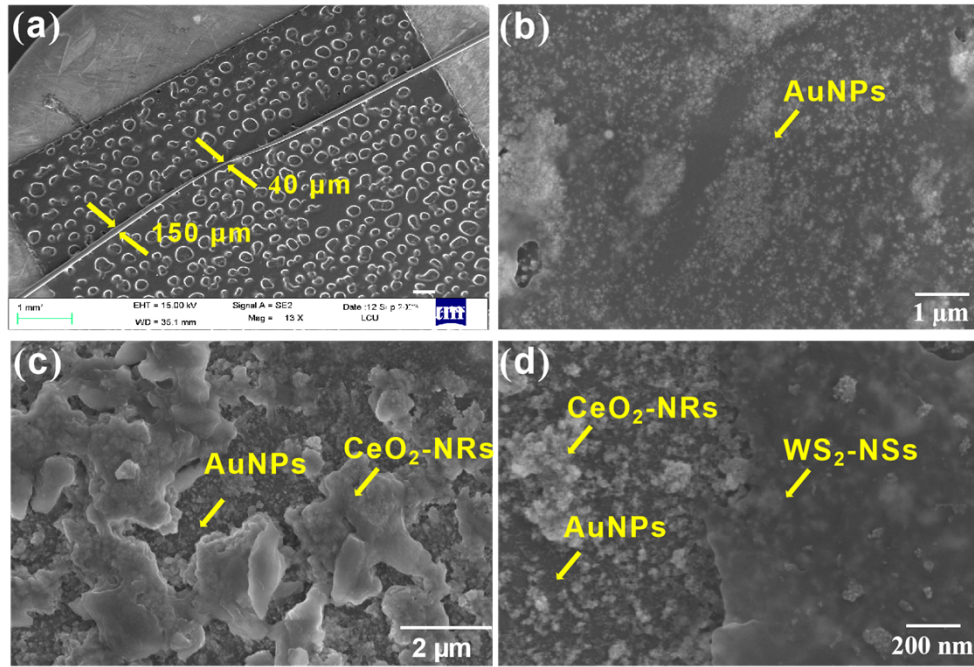


Fig. 8. (a) Images of the fiber structure under microscope; SEM images of (b) AuNPs-coated, (c) AuNPs/CeO₂-coated and (d) AuNPs/CeO₂/WS₂-NSs-coated fiber structure.

The microscope was used to characterize the WaveFlex fiber structure based on S-tapered and waist-expanded techniques. As can be seen from Fig. 8(a), the diameter of the waist-expanded ball was 150 μm, and the diameter of the taper area was 40 μm. Moreover, the fiber on both sides of the taper region had an obvious axial deviation. SEM was used to evaluate and characterize the nanomaterials that were functionalized on the fiber probe. In Fig. 8(b), it can be clearly seen that AuNPs are successfully attached to the fiber surface and that the dispersion of NPs is relatively uniform. Figure 8(c) showed the SEM information of CeO₂, in which CeO₂ with a layered structure was stacked on top of AuNPs. The SEM information of the immobilized AuNPs/CeO₂/WS₂ on the surface of the fiber probe is shown in Fig. 8(d). WS₂-NSs were successfully fixed on the fiber probe. The combination of the above two materials is conducive to enhancing the adhesion site of the antibodies and the performance of the sensor.

3.2. HbA1c solution and stability test

The developed Waveflex fiber probe was employed to detect HbA1c solutions at different concentrations. The test process was performed from low to high concentrations, and the sensor probe needed to be washed with PBS after each test. Because of the presence of HbA1c antibodies on the surface of the sensor probe, it will cause different RI changes in the external environment when the probe is placed in different concentrations of HbA1c solution. The RI change can be demonstrated by the change in transmitted intensity, as depicted in Fig. 9(a). Through the linear fitting of the transmitted intensity with the variation of HbA1c concentration, the sensitivity can be obtained:

$$I = -1.195 \times 10^{-5} C + 2.864 \times 10^4 \quad (1)$$

here, I represents the transmitted intensity, and C is the HbA1c concentration. The linear correlation fitting factor $R^2 = 0.973$, as shown in Fig. 9(b), indicating a good linear fit. Stability is a crucial metric for assessing the sensor probe. The transmission intensity of $1 \times$ PBS was

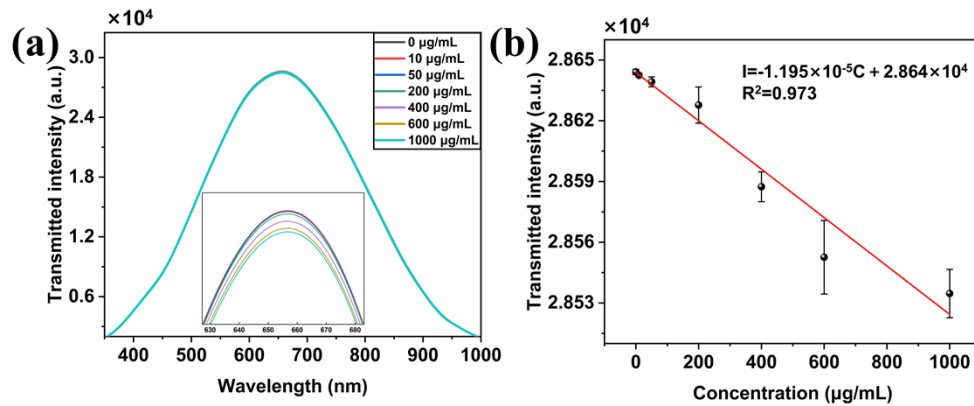


Fig. 9. The measurement results of the HbA1c sensor probe. (a) transmitted intensity; (b) linearity of the developed probe.

recorded ten-times with the developed fiber probe. The experiment's findings are displayed in Fig. 10. The Limit of detection (LoD), as an essential aspect to evaluate the sensor, is the lowest concentration that can be detected. The calculation method is the ration of three-times standard deviation ($SD = 0.66$) and sensitivity, and the LOD is obtained at $1.66 \mu\text{g/mL}$.

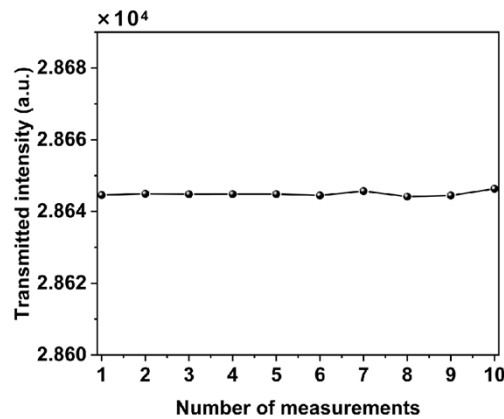


Fig. 10. Stability test of the fiber sensor probe.

3.3. Reproducibility and reusability test

Reproducibility and reusability are crucial criteria for evaluate the practical application capability of a sensor probe. The reproducibility test is to select three probes to test the same concentration and observe whether the sensing results are consistent. Three sensor probes were employed to test a $1000 \mu\text{g/mL}$ HbA1c solution, as shown in Fig. 11(a). The outcomes reveal that the sensing results of the three probes are highly consistent, which proves the good reproducibility of the prepared probes.

The same sensor probe was utilized to test the same concentration after 30 days to measure the stability over time. The probes were tested at $0 \mu\text{g/mL}$ and $1000 \mu\text{g/mL}$ HbA1c solutions, respectively. The same spectral transmitted intensity results in Fig. 11(b) demonstrate the reusability of the developed probes over time.

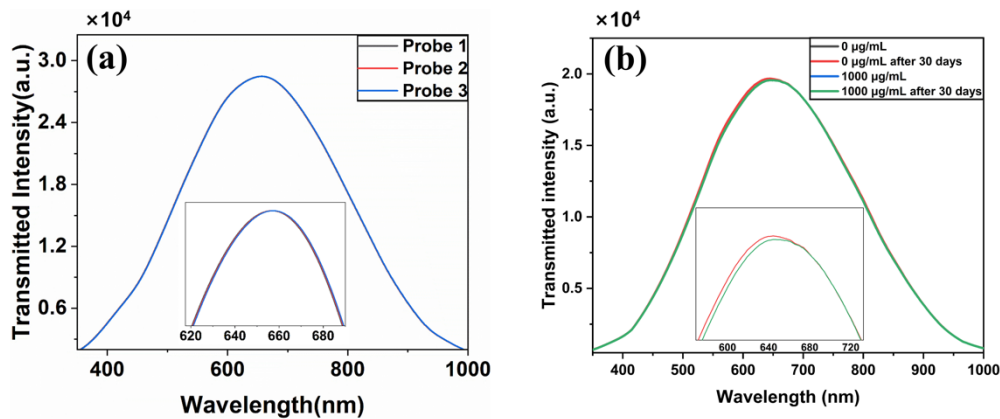


Fig. 11. Sensing performance analysis, (a) reproducibility, and (b) reusability test of fiber probe after 30 days.

3.4. pH and selectivity test

To verify the application capability of the developed sensor probes in different pH solution environments, PBS solutions with pH values of 3, 6, 10, and 13 were prepared by using acetic acid and KOH, respectively. The HbA1c solutions of 0 $\mu\text{g/mL}$ and 1000 $\mu\text{g/mL}$ were mixed with the solution with different pH values, respectively. The measurement's findings are displayed in Fig. 12(a). The variety of transmitted intensity is greatest when the pH value is 7.4. For other pH values in a solution environment, there is little or no change in spectral intensity. The strong acid or alkali environment causes the inactivation of antibodies, which affects the sensing performance. The maximum spectral intensity variation with a pH value of 7.4 demonstrates the potential application in human serum.

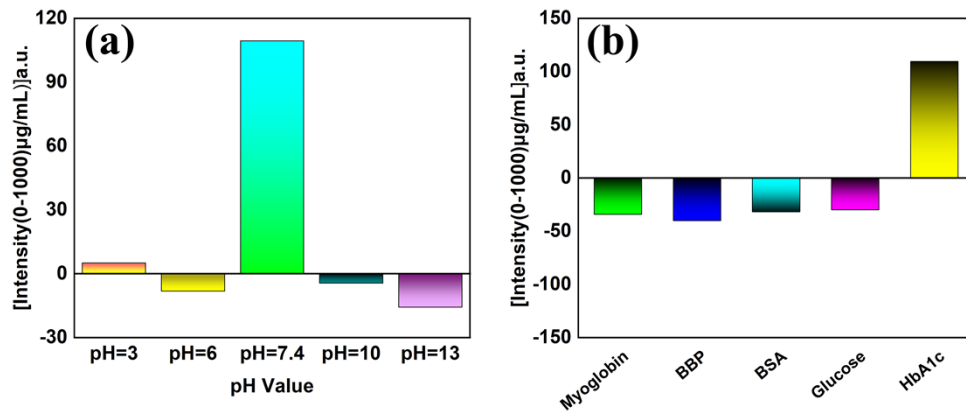


Fig. 12. (a) pH and (c) selectivity test of developed fiber sensor probe.

The unique recognition of the sensor probe is also an important parameter. The proposed probe must be insensitive to any substances except HbA1c. The myoglobin, BBP, BSA, glucose, and HbA1c solutions of 0 $\mu\text{g/mL}$ and 1000 $\mu\text{g/mL}$ were prepared to perform the selectivity test. The results in Fig. 12(b) show that the transmitted intensity changes the most when the detection sample is HbA1c. The presence of HbA1c antibodies on the probe makes the sensor probe

Table 1. Performance comparison of the proposed sensor with existing ones.

Mechanism	Materials used	Detection Range	Sensitivity	Detection limit	Ref.
Electrochemical	MWCNTs/AuNPs	0.186-2.004 g/dL	n.r. ^a	0.186 g/dL	[39]
Electrochemical	NF/MWCNT	31.2-500nM	n.r. ^a	4.2 nM	[40]
SPR	vinyl phenyl boronic acid (VPBA)	10-200 µg/mL	n.r. ^a	2.86 µg/mL	[41]
LSPR	AuNPs	0.09-2.35 g/L	n.r. ^a	0.03 g/L	[42]
Colorimetric	AuNPs	4%-14%	n.r. ^a	42.5 g/mL	[43]
LSPR	AuNPs/CeO ₂ -NRs/WS ₂ -NSs	0-1000 µg/mL	1.195×10^{-5} a.u./µg/mL	1.66 µg/mL	This work

^aNot reported

possess the ability to recognize HbA1c. Consequently, it can be concluded that the proposed sensor probe can be applied to human serum for the detection of HbA1c.

3.5. Evaluation of sensing performance

The developed HbA1c fiber biosensor based on the S-tapered and waist-expanded technique possesses the characteristics of high sensitivity, portability, low cost, and novelty. The performance is summarized in Table 1 of HbA1c biosensors based on different mechanisms. The compared results show that our proposed fiber biosensor for the detection of HbA1c has the advantages of high sensitivity, a broad detection range, and a good LoD. The idea of developing HbA1c biosensors based on novel fiber structures and nanomaterial enhancement techniques has been fully proven.

4. Conclusion

In this work, a plasmonic fiber HbA1c sensor based on the S-tapered and waist-expanded technique was proposed for the first time. AuNPs were first fixed on the fiber probe in order to activate the LSPR to achieve the signal enhancement.

CeO₂-NRs capable of strong metal-carrier interactions with AuNPs were then immobilized on the sensor probe surface to enhance the cascade of CeO₂-NRs and AuNPs. The combination of CeO₂-NRs with the layered fold structure of WS₂-NSs can form a dense integrated composite structure on the probe surface, which can increase the site of biological antibodies. The sensor probe possesses the ability for specific selection by functionalizing the HbA1c antibodies on the surface of the probe. The sensitivity and LoD were obtained to be 1.195×10^{-5} a.u./µg/mL and 1.66 µg/mL by measuring different concentrations of HbA1c. The good linear fitting was observed to be 0.973 over a linear range of 0-1000 µg/mL. Moreover, reproducibility, reusability, selectivity, and pH test experiments were performed to evaluate the sensor probe. The results demonstrate that the proposed plasmonic fiber HbA1c sensor has the potential for diabetes mellitus detection.

Natural Science Foundation of Shandong Province (Grant No. ZR2022QF137, ZR2020QC061); Double- Hundred Talent Plan of Shandong Province, China; Special Construction Project Fund for Shandong Province Taishan Mountain Scholars; Liaocheng University (318052205, 318052341); Science and Technology Support Plan for Youth Innovation of Colleges and Universities of Shandong Province of China (2022KJ107).

Funding. Natural Science Foundation of Shandong Province (ZR2020QC061, ZR2022QF137); Double- Hundred Talent Plan of Shandong Province, China; Special Construction Project Fund for Shandong Province Taishan Mountain Scholars; Liaocheng University (318052205, 318052341); Science and Technology Support Plan for Youth Innovation of Colleges and Universities of Shandong Province of China (2022KJ107).

Disclosures. The authors declare no conflicts of interest.

Data availability. Data underlying the results presented in this paper are not publicly available at this time but may be obtained from the authors upon reasonable request.

References

1. H. Sun, P. Saeedi, S. Karuranga, *et al.*, "IDF Diabetes Atlas: Global, regional and country-level diabetes prevalence estimates for 2021 and projections for 2045," *Diabetes Res. Clin. Pract.* **183**, 109119 (2022).
2. J. Chaki, S. T. Ganesh, S. K. Cidham, *et al.*, "Machine learning and artificial intelligence based diabetes mellitus detection and self-management: A systematic review," *Journal of King Saud University-Computer and Information Sciences* **34**(6), 3204–3225 (2022).
3. A. Amer Diabet, "Diagnosis and Classification of Diabetes Mellitus," *Diabetes Care* **36**(Supplement_1), S67–S74 (2013).
4. J. F. Yale, G. Bakris, B. Cariou, *et al.*, "Efficacy and safety of canagliflozin in subjects with type 2 diabetes and chronic kidney disease," *Diabetes, Obes. Metab.* **15**(5), 463–473 (2013).
5. M. Kropp, O. Golubnitschaja, A. Mazurakova, *et al.*, "Diabetic retinopathy as the leading cause of blindness and early predictor of cascading complications-risks and mitigation," *Epma Journal* **14**(1), 21–42 (2023).
6. Z. X. Chen, L. M. Shao, M. F. Jiang, *et al.*, "Interpretation of HbA1c lies at the intersection of analytical methodology, clinical biochemistry and hematology (Review)," *Exp. Ther. Med.* **24**(6), 707 (2022).
7. E. Papathanassiou, A. I. Papaioannou, I. Papanikolaou, *et al.*, "Glycated hemoglobin (HbA1c) as a predictor of outcomes during acute exacerbations of chronic obstructive pulmonary disease," *Copd-Journal of Chronic Obstructive Pulmonary Disease* **18**(2), 219–225 (2021).
8. A. Jayedi, S. Zeraattalab-Motlagh, B. Jabbarzadeh, *et al.*, "Dose-dependent effect of carbohydrate restriction for type 2 diabetes management: a systematic review and dose-response meta-analysis of randomized controlled trials," *Am. J. Clin. Nutr.* **116**(1), 40–56 (2022).
9. R. A. Vigersky and C. McMahon, "The relationship of hemoglobin A1C to time-in-range in patients with diabetes," *Diabetes Technol. Ther.* **21**(2), 81–85 (2019).
10. E. Noviana, S. Siswanto, and A. A. M. Budi Hastuti, "Advances in nanomaterial-based biosensors for determination of glycated hemoglobin," *Curr. Top. Med. Chem.* **22**(27), 2261–2281 (2022).
11. I. Conget, M. S. Kirkman, D. C. Cao, *et al.*, "Identifying insulin treatment responders with a composite measure: beyond HbA1c < 7% in patients with type 2 diabetes," *Curr. Med. Res. Opin.* **34**(2), 329–336 (2018).
12. K. Rytter, K. P. Madsen, H. U. Andersen, *et al.*, "Associations between insulin pump self-management and HbA1c in type 1 diabetes," *Diabetic Med.* **40**(6), 1 (2023).
13. H. Lin and J. Yi, "Current Status of HbA1c Biosensors," *Sensors* **17**(8), 1798 (2017).
14. A. Ahmadi, S. Kabiri, and K. Omidfar, "Advances in HbA1c biosensor development based on field effect transistors: a review," *IEEE Sens. J.* **20**(16), 1 (2020).
15. K. S. Ahn, J. H. Lee, J. M. Park, *et al.*, "Luminol chemiluminescence biosensor for glycated hemoglobin (HbA1c) in human blood samples," *Biosens. Bioelectron.* **75**, 82–87 (2016).
16. M. Thapa and Y. S. Heo, "Label-free electrochemical detection of glucose and glycated hemoglobin (HbA1c)," *Biosens. Bioelectron.* **221**, 114907 (2023).
17. D. W. Mulder, M. M. Phiri, and B. C. Vorster, "Gold nanostar colorimetric detection of fructosyl valine as a potential future point of care biosensor candidate for glycated haemoglobin detection," *Biosensors* **9**(3), 100 (2019).
18. M. Y. Li, R. Singh, C. Marques, *et al.*, "2D material assisted SMF-MCF-MMF-SMF based LSPR sensor for creatinine detection," *Opt. Express* **29**(23), 38150–38167 (2021).
19. R. Singh, S. Kumar, F. Z. Liu, *et al.*, "Etched multicore fiber sensor using copper oxide and gold nanoparticles decorated graphene oxide structure for cancer cells detection," *Biosens. Bioelectron.* **168**, 112557 (2020).
20. X. Liu, R. Singh, M. Li, *et al.*, "Plasmonic sensor based on offset-splicing and waist-expanded taper using multicore fiber for detection of Aflatoxins B1 in critical sectors," *Opt. Express* **31**(3), 4783–4802 (2023).
21. S. Kumar, Z. Guo, R. Singh, *et al.*, "MoS₂ functionalized multicore fiber probes for selective detection of shigella bacteria based on localized plasmon," *J. Lightwave Technol.* **39**(12), 4069–4081 (2021).
22. M. S. Soares, L. C. B. Silva, C. A. F. Vidal, *et al.*, "Label-free plasmonic immunosensor for cortisol detection in a D-shaped optical fiber," *Biomed. Opt. Express* **13**(6), 3259–3274 (2022).
23. A. A. Rifat, R. Ahmed, F. R. M. Yetisen, *et al.*, "Photonic crystal fiber based plasmonic sensors," *Sens. Actuators, B* **243**, 311–325 (2017).
24. S. Choudhary, F. Esposito, A. Sansone, *et al.*, "Lossy mode resonance sensors in uncoated optical fiber," *IEEE Sens. J.* **23**(14), 15607–15613 (2023).
25. F. Esposito, A. Stancalie, A. Srivastava, *et al.*, "The impact of gamma irradiation on optical fibers identified using long period gratings," *J. Lightwave Technol.* **41**(13), 4389–4396 (2023).
26. F. Esposito, S. Campopiano, and A. Iadicco, "Miniaturized strain-free fiber Bragg grating temperature sensors," *IEEE Sens. J.* **22**(17), 16898–16903 (2022).
27. J. W. Feng, J. J. Gao, W. Yang, *et al.*, "LSPR optical fiber sensor based on 3D gold nanoparticles with monolayer graphene as a spacer," *Opt. Express* **30**(6), 10187–10198 (2022).
28. M. Yang, Y. Y. Chen, H. T. Wang, *et al.*, "Solvothetral preparation of CeO₂ nanoparticles-graphene nanocomposites as an electrochemical sensor for sensitive detecting pentachlorophenol," *Carbon Lett.* **32**(5), 1277–1285 (2022).

29. Y. Kang, Y. H. Zhang, Q. Shi, *et al.*, "Highly efficient $\text{Co}_3\text{O}_4/\text{CeO}_2$ heterostructure as anode for lithium-ion batteries," *J. Colloid Interface Sci.* **585**, 705–715 (2021).
30. K. H. Han, Y. Wang, S. Wang, *et al.*, "Narrowing band gap energy of CeO_2 in $(\text{Ni}/\text{CeO}_2)/\text{SiO}_2$ catalyst for photothermal methane dry reforming," *Chem. Eng. J.* **421**, 129989 (2021).
31. M. Li, J. Fang, C. Wang, *et al.*, " $\text{CePO}_4/\text{CeO}_2$ heterostructure and enzymatic action of $\text{D-Fe}_2\text{O}_3$ co-amplify luminol-based electrochemiluminescence immunosensor for NSE detection," *Biosens. Bioelectron.* **214**, 114516 (2022).
32. W. Cheng, Z. Lin, L. Zhao, *et al.*, " $\text{CeO}_2/\text{MXene}$ heterojunction-based ultrasensitive electrochemiluminescence biosensing for BCR-ABL fusion gene detection combined with dual-toehold strand displacement reaction for signal amplification," *Biosens. Bioelectron.* **210**, 114287 (2022).
33. Y. L. Zhou, H. S. Yin, and S. Y. Ai, "Applications of two-dimensional layered nanomaterials in photoelectrochemical sensors: A comprehensive review," *Coord. Chem. Rev.* **447**, 214156 (2021).
34. Y. Guo, S. Mei, K. Yuan, *et al.*, "Low-temperature CO_2 methanation over CeO_2 -supported Ru single atoms, nanoclusters, and nanoparticles competitively tuned by strong metal-support interactions and h-spillover effect," *ACS Catal.* **8**(7), 6203–6215 (2018).
35. G. Li, R. Singh, S. Guo, *et al.*, " Nb_2CT_x MXene-assisted double S-tapered fiber-based LSPR sensor with improved features for tyramine detection," *Appl. Phys. Lett.* **122**(8), 1 (2023).
36. A. Dhali and W. Self, "Cerium oxide nanoparticles: a brief review of their synthesis methods and biomedical applications," *Antioxidants* **7**(8), 97 (2018).
37. N. S. Heo, C. H. Kwak, H. Lee, *et al.*, "Simple diagnosis of HbA1c using the dual-plasmonic platform integrated with LSPR and SERS," *J. Cryst. Growth* **469**, 154–159 (2017).
38. P. Bhattacharyya and D. Acharyya, "Impact of device configurations on sensing performance of WS_2 -based gas sensors: a review," *IEEE Sens. J.* **21**(20), 22414–22425 (2021).
39. K. Ponsanti, N. Ngernyung, B. Tangnorawich, *et al.*, "A novel electrochemical-biosensor microchip based on MWCNTs/AuNPs for detection of glycated hemoglobin (HbA1c) in diabetes patients," *J. Electrochem. Soc.* **169**(3), 037520 (2022).
40. M. Thiruppathi, J.-F. Lee, C. C. Chen, *et al.*, "A disposable electrochemical sensor designed to estimate glycated hemoglobin (HbA1c) level in whole blood," *Sens. Actuators, B* **329**, 129119 (2021).
41. M. Çalışır, M. Bakhshpour, H. Yavuz, *et al.*, "HbA1c detection via high-sensitive boronate based surface plasmon resonance sensor," *Sens. Actuators, B* **306**, 127561 (2020).
42. R. Thea, D. Onna, M. P. Kreuzer, *et al.*, "Label-free nanostructured sensor for the simple determination of glycosylated hemoglobin (HbA1c)," *Sens. Actuators, B* **297**, 126722 (2019).
43. S. H. Ang, T. M. Thevarajah, P. M. Woi, *et al.*, "A lateral flow immunosensor for direct, sensitive, and highly selective detection of hemoglobin A1c in whole blood," *J. Chromatogr. B: Anal. Technol. Biomed. Life Sci.* **1015–1016**, 157–165 (2016).